Ultrasound in Med. & Biol., Vol. 49, No. 1, pp. 62−71, 2023

0301-5629/$ - see front matter

https://doi.org/10.1016/j.ultrasmedbio.2022.07.014

● *Original Contribution*

INITIAL ASSESSMENT OF BOILING HISTOTRIPSY FOR MECHANICAL ABLATION OF *EX VIVO* HUMAN PROSTATE TISSUE

Vera A. Khokhlova,[*,†] Pavel B. Rosnitskiy,[†] Sergey A. Tsysar,[†] Sergey V. Buravkov,[‡,§] Ekaterina M. Ponomarchuk,[†] Oleg A. Sapozhnikov,[*,†] Maria M. Karzova,[†] Tatiana D. Khokhlova,[¶] Adam D. Maxwell,[‖] Yak-Nam Wang,[*] Alexey V. Kadrev,[#,**] Andrey L. Chernyaev,[§,††] Valery P. Chernikov,[§] Dmitriy A. Okhobotov,[#] Armais A. Kamalov,[#] and George R. Schade[‖]

[*] Center for Industrial and Medical Ultrasound, Applied Physics Laboratory, University of Washington, Seattle, Washington, USA; [†] Physics Faculty, Lomonosov Moscow State University, Moscow, Russia; [‡] Laboratory of Cell Image Analysis, Faculty of Fundamental Medicine, Lomonosov Moscow State University, Moscow, Russia; [§] Research Institute of Human Morphology, Moscow, Russia; [¶] Division of Gastroenterology, Department of Medicine, University of Washington School of Medicine, Seattle, Washington, USA; [‖] Department of Urology, University of Washington School of Medicine, Seattle, Washington, USA; [#] Medical Research and Educational Center, Department of Urology and Andrology, Lomonosov Moscow State University, Moscow, Russia; [**] Diagnostic Ultrasound Division, Russian Medical Academy of Continuous Professional Education, Moscow, Russia; and [††] Pulmonology Scientific Research Institute, Moscow, Russia

(*Received* 2 *April* 2022; *revised* 27 *July* 2022; *in final form* 31 *July* 2022)

Abstract—Boiling histotripsy (BH) is a focused ultrasound technology that uses millisecond-long pulses with shock fronts to induce mechanical tissue ablation. The pulsing scheme and mechanisms of BH differ from those of cavitation cloud histotripsy, which was previously developed for benign prostatic hyperplasia. The goal of the work described here was to evaluate the feasibility of using BH to ablate fresh *ex vivo* human prostate tissue as a proof of principle for developing BH for prostate applications. Fresh human prostate samples (N = 24) were obtained via rapid autopsy (<24 h after death, institutional review board exempt). Samples were analyzed using shear wave elastography to ensure that mechanical properties of autopsy tissue were clinically representative. Samples were exposed to BH using 10- or 1-ms pulses with 1% duty cycle under real-time B-mode and Doppler imaging. Volumetric lesions were created by sonicating 1−4 rectangular planes spaced 1 mm apart, containing a grid of foci spaced 1−2 mm apart. Tissue then was evaluated grossly and histologically, and the lesion content was analyzed using transmission electron microscopy and scanning electron microscopy. Observed shear wave elastography characterization of *ex vivo* prostate tissue (37.9 ± 22.2 kPa) was within the typical range observed clinically. During BH, hyperechoic regions were visualized at the focus on B-mode, and BH-induced bubbles were also detected using power Doppler. As treatment progressed, hypoechoic regions of tissue appeared, suggesting successful tissue fractionation. BH treatment was twofold faster using shorter pulses (1 ms vs. 10 ms). Histological analysis revealed lesions containing completely homogenized cell debris, consistent with histotripsy-induced mechanical ablation. It was therefore determined that BH is feasible in fresh *ex vivo* human prostate tissue producing desired mechanical ablation. The study supports further work aimed at translating BH technology as a clinical option for prostate ablation. (E-mail: verak2@uw.edu) **© 2022 World Federation for Ultrasound in Medicine & Biology. All rights reserved.**

Key Words: **Boiling histotripsy, High-intensity focused ultrasound, Prostate.**

INTRODUCTION

Histotripsy is a developmental high-intensity focused ultrasound (HIFU) technology that induces non-thermal mechanical tissue ablation (Parsons et al. 2006; Khokhlova et al. 2011, 2015; Lin et al. 2014; Eranki et al. 2018; Xu et al. 2021). Compared with existing clinical thermal HIFU regimes, histotripsy delivers sequences of shorter pulses (from microseconds to a few milliseconds) of higher acoustic power (10- to 100-fold) at low duty cycle (<1%). Central to the mechanism of histotripsy is formation of vapor/gas bubbles at the focus that leads to

Address correspondence to: Vera A. Khokhlova, Center for Industrial and Medical Ultrasound, Applied Physics Laboratory, University of Washington, 1013 NE 40th Street, Seattle, WA 98105, USA E-mail: verak2@uw.edu

mechanical effects through ultrasound−bubble interactions (Maxwell et al. 2011; Simon et al. 2012; Pahk et al. 2017). The presence of these bubbles produces hyperechogenicity during each pulse, and the ensuing mechanical destruction of tissue eliminates tissue scatterers, producing a hypoechoic cavity as treatment completes (Wang et al. 2009; Khokhlova et al. 2019a). Collectively, this allows for real-time targeting, treatment monitoring, and evaluation of treatment outcomes on B-mode ultrasound, which provides minimal real-time feedback with purely thermal HIFU. Additionally, because of the non-thermal mechanism and rapidity of bio-effects, histotripsy minimizes heat sinking and thermal spread that can limit the consistency and precision of HIFU thermal ablation. In general, the precision of thermal ablative techniques is highly dependent on the target tissue, the thermal dose, and the area over which the thermal dose is applied (Elhelf et al. 2018; Gschwend et al. 2021). However, it is generally accepted that a margin of at least 5 mm beyond a tumor region is needed to provide less frequent recurrence given the limitations of contemporary tumor localization techniques (*e.g.,* magnetic resonance imaging [MRI]). As a result, histotripsy may offer a strategy to improve HIFU ablation.

Accordingly, histotripsy has been under development for several clinical applications including ablation of the prostate for both benign prostatic hyperplasia (BPH) and prostate cancer (PCa) (Hempel et al. 2011; Schade et al. 2012a, 2012b; Khokhlova et al. 2019b; Dubinsky et al. 2020;). Initial prostate studies used “cavitation cloud” histotripsy, which relies on microsecond-duration pulses and very high peak rarefactive (negative) pressures to induce microbubbles at the focus through shock scattering (Hall et al. 2009; Maxwell et al. 2011). Early pre-clinical work showed promise, and the technology proceeded to phase 1 clinical trials for treatment of BPH using the Vortx Rx device (HistoSonics, Ann Arbor, MI, USA) through a transperineal approach. Though men demonstrated a significant subjective improvement in their lower urinary tract symptoms for up to 6 months after treatment, there were no objective improvements in prostate volume, flow rate or post-void residual (Schuster et al. 2018). The relatively small boney acoustic window and significant depth of the prostate for the transperineal approach, combined with the device’s pulse parameters, may have limited the ability to produce significant ablation of BPH.

Our group has been developing an alternative histotripsy regime, termed *boiling histotripsy* (BH). BH uses milliseconds-long (<20 ms) pulses and non-linear propagation effects to generate high-amplitude shock fronts in acoustic pressure waveform at the focus (Khokhlova et al. 2011). Super-efficient shock-wave focusing and shock-induced heating result in formation of a millimeter-sized vapor bubble at the focus within each pulse (Canney et al. 2010). Interaction of subsequent shock fronts with this bubble produces mechanical tissue ablation with negligible thermal effects through pre-focal cavitation, acoustic atomization, and micro-fountaining (Khokhlova et al. 2011; Maxwell et al. 2011; Simon et al. 2012; Pahk et al. 2017). Ultrasonic atomization, that is, emission of fine droplets, and micro-fountain formation are well-known phenomena that occur when a focused ultrasound wave propagating in liquid encounters an interface with air (Simon et al. 2012). Focal waveforms in BH fields are asymmetric and have very high peak positive pressures following the shock fronts. When reflected from the pressure-release boundary of the vapor-filled boiling bubble, the wave changes polarity, which leads to creation of very high negative pressures in tissue in front of the bubble. This results in pre-focal cavitation and weakening or partial disintegration of the tissue. The acoustic radiation force caused by the BH beam pushes this tissue inside the vapor cavity, forming a miniature acoustic fountain of tissue fragments, and consequent atomization occurs inside the vapor bubble. The process is repeated with each incident pulse, resulting in complete tissue liquefaction.

The BH method therefore relies on shock amplitude instead of peak rarefactional pressure and has lower power requirements, which may make it more conducive to transducer miniaturization and a transrectal application for prostate indications. In the work described here, building on prior experiments (Khokhlova et al. 2019b), we evaluated the feasibility of using BH to ablate fresh *ex vivo* human prostate tissue as a proof of principle for developing BH for prostate applications.

METHODS

Fresh human prostate tissue samples (N = 24) were obtained via rapid autopsy (<24 h after death, institutional review board exempt). The sizes of samples varied from 4 to 15 cm^3. Tissue samples were placed in phosphate-buffered saline solution and de-gassed in a desiccant chamber for at least 1 h with residual pressure <0.1 bar. For all BH experiments, the samples then were embedded in 1% agarose gel (N = 16). For shear wave elastography measurements, the samples (N = 8) were kept in de-gassed water to perform imaging.

Shear wave elastography imaging tissue characterization

Mechanical properties of the autopsy prostate tissue were analyzed in N = 8 samples using shear wave elastography (SWE) imaging to ensure that no significant change in tissue stiffness occurred within 24 h after death. To reduce artifacts at the edges of tissue samples, which were much stronger when they were embedded in agarose gel, the measurements were performed in a container filled with de-gassed water. Each tissue sample was placed in water on an absorbing silicone rubber layer, positioned so that the imaging was performed from the same direction as the BH exposure, and the areas of interest for quantitative measurement were chosen in the middle of the samples away from the artifact areas. An Aixplorer ultrasound system with gray-scale ultrasound imaging and SWE (SuperSonic Imagine, Aix-en-Provence, France) and a linear probe SL15-4 with an effective bandwidth of 4 to 15 MHz were used in the measurements.

Settings were optimized for depth of penetration using a thyroid gland pre-set with an elasticity scale of 100 kPa. SWE images were obtained and recorded in the imaging plane through the center of each sample. For each measurement, the transducer was maintained in a steady position for 4 s until the images stabilized. In each image, the elastic (Young's) modulus was measured within three 4-mm-diameter circular regions of interest centered at depths of 6, 12, and 18 mm in the sample. Each Young's modulus measurement was performed three times, and the average value was recorded. For analysis, the values obtained in all 24 measurements were used.

Boiling histotripsy sonication

Agarose-embedded prostate tissue samples (N = 16) were placed in a custom holder submerged in de-gassed water and attached to a 3-D positioning system (Precision Acoustics, Dorchester, UK), as illustrated in Figure 1a. BH pulses were delivered using a 1.5-MHz custom-made transducer 80 mm in diameter and 60 mm in focal length, with a 24-mm diameter central opening (Fig. 1b).

To ensure successful tissue liquefaction in all samples, the transducer was operated at the highest driving voltage of 240 V provided by a custom-made electronic driving system similar to that described and characterized in our previous study (Maxwell et al. 2017). Acoustic power of the transducer and *in situ* focal pressures were estimated using measurement-based non-linear modeling with an equivalent single-element source as a boundary condition (Rosnitskiy et al. 2017). Pressure distributions were measured and reconstructed from acoustic holography measurements (Sapozhnikov et al. 2015) performed in a plane between the transducer and the focus using a calibrated hydrophone (HNA-0400, 1 mV/kPa at 1.5 MHz; Onda Corp., Sunnyvale, CA, USA) at low driving voltage (3 V). Geometrical parameters of an equivalent single-element source with a central opening and uniform distribution of the vibrational velocity on its surface were defined so that its axial pressure amplitude distribution matched the focal lobe (above the −6-dB level) of the corresponding experimentally obtained axial distributions as illustrated in Figure 2a. Then, assuming linear dependence of the source pressure on the driving voltage (Maxwell et al. 2017), non-linear simulations were performed for the equivalent source at the operational output (240 V) using a HIFU-beam software (Yuldashev et al. 2021). Simulations were performed in a layered medium "water−prostate" with the focus located 1 cm deep inside the prostate (Fig. 2b). Focal waveform was also derated from simulations in water, performed at lower voltage to compensate for attenuation in tissue (Khokhlova et al. 2011).

The following parameters were used in acoustic simulations in water and tissue, respectively: sound speed 1490.6 and 1559.5 m/s, density 997 and 1045 kg/m^3, non-linear parameter 3.5 and 4.8, thermoviscous absorption (sound diffusivity) 4.33×10^{-6} m^2/s, with additional absorption in tissue of 1.2 dB/cm at 1.5 MHz with a power law of 1.1 (Duck 1990). The aperture of the equivalent source was 65.8 mm, the focal length 56 mm and the central opening aperture 20 mm; the characteristic source pressure amplitude that corresponded to a 3-V driving voltage was 10 kPa. An acoustic output of 240 V used in BH experiments corresponded to a 734-W acoustic power of the equivalent source, 0.8-MPa characteristic pressure amplitude or 21-W/cm^2 intensity on its surface. Peak pressures in the focal waveform, directly simulated and derated from simulations in water, were P_+/P_- = 122/−22 MPa, and the shock amplitude was 135 MPa (Fig. 2c).

Boiling histotripsy exposures were delivered to a rectangular grid containing 2−11 foci in the transverse directions along the scanning plane (Fig. 3a). Depending on the size and geometry of the samples, foci were spaced 1−2 mm apart. Volumetric lesions were obtained by sonicating 1−4 scanning planes with 1 mm between them. Two BH exposure protocols with the same peak acoustic power were evaluated (N = 8 samples each). For both protocols, bubbles were detected at the focus by B-mode and Doppler imaging in all treatments, 100% of the treatment time. The first protocol (Fig. 3b) used pulses 10 ms in duration delivered at 1% duty cycle, 20−40 pulses per focus. This is the "standard" BH protocol that has been used for treatments of different tissues (Wang et al. 2018b; Khokhlova et al. 2019a), including an initial pilot study in human prostate (Khokhlova et al. 2019b). The second protocol used shorter pulses of 1-ms duration, 1% duty cycle and 75−150 pulses per sonication point, with the aim of accelerating the treatment (Fig. 3c).

In the first N = 4 samples tested for each BH pulse duration regime (N = 8 total), different spacing and number of pulses per focus were assessed to optimize BH treatments. Focus spacing and the minimum number of

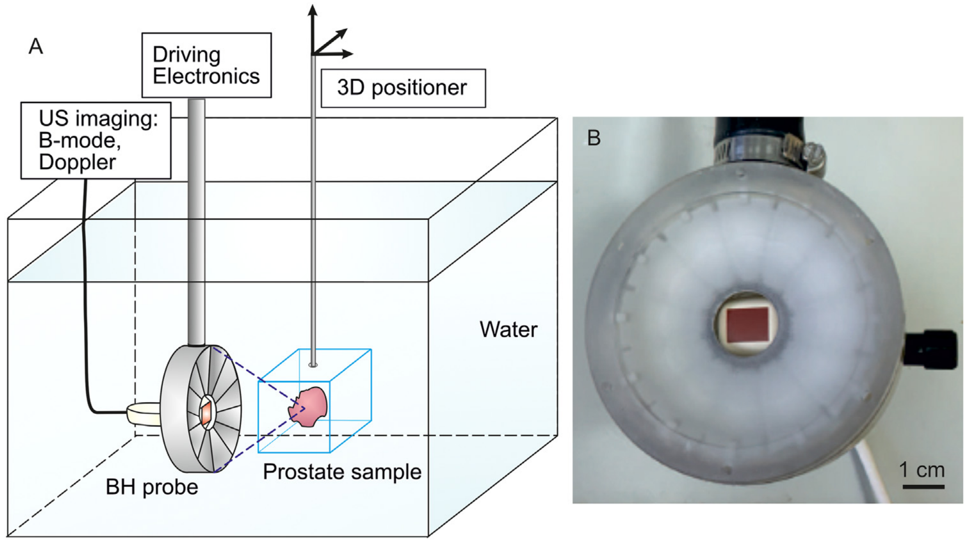

Fig. 1. (a) Experimental arrangement for boiling histotripsy (BH) treatment of *ex vivo* tissue under real time ultrasound imaging. (b) Photograph of the BH transducer with the P7-4 imaging probe placed in its central opening.

pulses needed to produce uniformly liquefied lesions were selected. Subsequently, N = 4 samples (N = 8 total) were treated for each BH pulse duration with the following BH sonication parameters: 1-mm spacing between the treatment foci and between the sonication planes; 30 pulses per focus for 10-ms pulses and 150 pulses per focus for 1-ms pulses.

Real-time-imaging feedback of the BH sonications and monitoring of the BH treatments were performed using a Verasonics V1 Ultrasound Engine (Kirkland, WA, USA). A P7-4 ATL probe operating in B-mode/power Doppler was placed within the central opening of the BH transducer (Fig. 1a, 1b). Doppler sequences were triggered by the BH driving electronics to generate images immediately after the end of each BH pulse (Li et al. 2014). B-Mode images were also collected after the exposure to evaluate the outcome of the treatment.

Specimen processing

After the initial N = 4 "optimization" BH exposures for each pulse duration regime, the samples were bisected for gross evaluation of lesion formation. Subsequently, for the optimized pulse parameters, N = 2 samples per pulse duration regime were formalin-fixed after BH exposures and processed for histologic assessment with Masson's trichrome staining. Additionally, N = 2 samples for each regime were bisected for gross evaluation, and then the lesion content was collected for ultrastructural analysis using transmission electron microscopy (TEM) and scanning electron microscopy (SEM).

RESULTS

Observed SWE imaging characterization of prostate tissue specimens was within the typical range observed

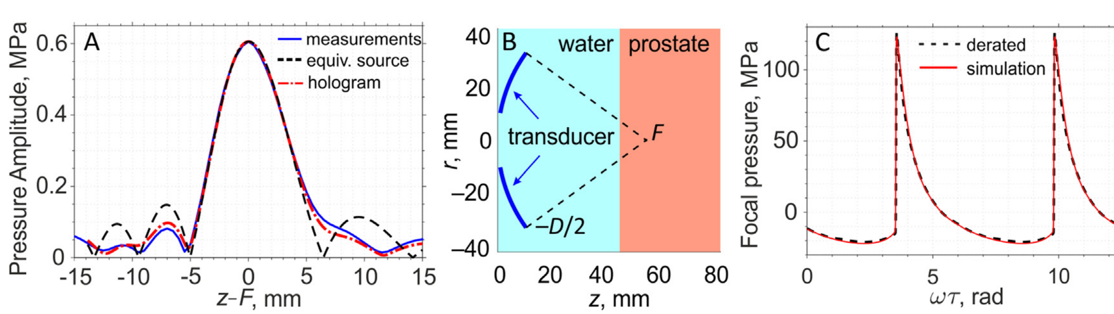

Fig. 2. (a) Axial pressure amplitude distribution reconstructed from acoustic holography measurements (*dashed−dotted curve*), directly measured by a hydrophone (*solid curve*), and simulated for an equivalent single-element source (*dashed curve*) at a low transducer driving voltage of 3 V. (b) Geometry of non-linear simulations for the equivalent source transducer in a "water−prostate" layered medium with the focus located 1 cm deep in tissue at the boiling histotripsy driving voltage of 240 V. (c) Two cycles of the focal waveform obtained from direct non-linear simulations (b) (*solid curve*) and derated from simulations in free field in water (*dashed curve*).

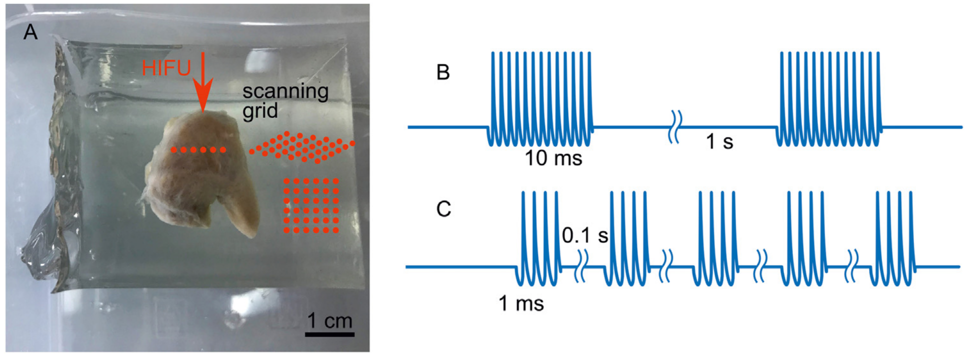

Fig. 3. (a) Tissue samples embedded in transparent gel and scheme of the scanning grid. (b, c) Diagrams of time sequences for (b) 10-ms long pulses and (c) 1-ms long pulses with 1% duty cycle. HIFU = high-intensity focused ultrasound

clinically (Barr et al. 2017). Specifically, the measured Young's moduli ranged from 11.9−91.7 kPa, with a mean ± standard deviation (SD) of 37.9 ± 22.2 kPa (Table 1). A representative photograph of an *ex vivo* prostate tissue sample with evidence of BPH and example B-mode and SWE images illustrating the range of tissue stiffness are provided in Figure 4.

The duration of BH treatments varied from 5 to 33 min for 1-ms pulses and from 10 to 60 min for 10-ms pulses, depending on the number of sonication points in one layer (2−11) and the number of layers (1−4). The geometry of the sonication grid was chosen with respect to the size and shape of the samples. In all treatments, hyperechoic regions were visualized during BH sonications at the focus on B-mode (Fig. 5a), and BH-induced bubbles were also detected using power Doppler mode (Fig. 5b). These areas persisted for at least 10−15 min after the BH exposure. As treatment progressed, hypoechoic regions of tissue appeared, suggesting successful tissue fractionation and liquefaction of the lesion content (Fig. 5c). On gross inspection of BH-treated tissue (Fig. 5d), lesions contained liquefied regions of a homogeneous suspension consistent with mechanical fractionation of tissue. As expected, treatment with a higher "dose" of 100 pulses, indicated by *yellow dots* in Fig. 5d, produced larger lesions compared with treatment with 30 pulses per focus, depicted by *blue dots.*

On gross inspection, in lesions produced with longer pulses (10 ms vs. 1 ms), slightly whitened tissue appeared around the lesion cavity (Fig. 6b), which may indicate some thermal effect on the surrounding tissues (Fig. 6a, 6b). Such color change is a known effect of thermal treatment of tissue. Above a specific thermal dose, tissue proteins will denature and coagulate. The changes in protein conformation and coagulation result in a color change in addition to an increase in opacity (Wang et al. 2018a; Park et al. 2019; Zhou et al. 2021).

The resulting lesion volumes closely approximated the rectangular geometry of the planned sonication grid for all treatments. With 10-ms pulses, all dimensions were ~1.5 mm larger than the grid size, and with 1-ms pulses, the dimensions were ~1 mm larger than the grid size. This expansion was expected and is consistent with the known focal lesion size (for each pulse duration) extending out from centers of the grid points at the lesion margins. Lesion evaluation performed grossly revealed that tissue was fully liquefied within the sonicated volumes.

On histological analysis, lesions containing homogenized cell debris were observed for both 1- and 10-ms pulses, consistent with histotripsy-induced mechanical ablation of glandular elements (Fig. 6). BH treatment with both pulse lengths resulted in uniform tissue homogenization containing <50-μm tissue fragments centrally. However, the use of shorter 1-ms pulses (with the same 1% duty cycle) required a larger number of pulses per focus compared with the use of 10-ms pulses (150 vs. 30, respectively) to achieve complete ablation, but resulted in a two-fold acceleration of the treatment. The treatment speed

Table 1. Shear wave elastography-measured Young's moduli (kPa) in three locations of eight *ex vivo* human prostate tissue samples

Location	Sample								
	1	2	3	4	5	6	7	8	Total
Proximal	24.5	27.7	20.8	11.9	45.5	18.4	80.6	34.8	
Central	29.8	23.6	12.6	19.8	47.8	16.6	82.7	55.2	
Distal	40.7	38.4	24.3	26.7	59.6	21.9	54	91.7	
Mean (SD)	31.7 (6.7)	29.9 (6.3)	19.2 (4.9)	19.4 (6.0)	51.0 (6.2)	19.0 (2.2)	72.4 (13.1)	60.6 (23.5)	37.9 (22.2)

SD = standard deviation.

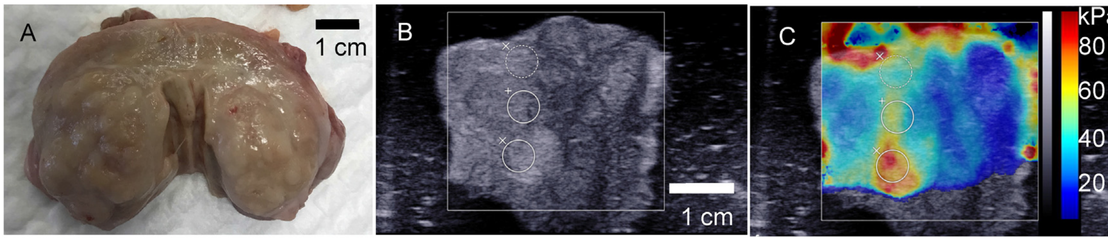

Fig. 4. (a) Photograph of an *ex vivo* human prostate tissue sample with evident presence of benign prostatic hyperplasia used in boiling histotripsy experiments. (b, c) Representative B-mode (b) and shear wave elastography (c) images of a prostate sample revealing a tissue stiffness (Young's modulus) ranging from 30−75 kPa.

evaluated grossly was 9 ± 1.7 mm^3/min for 1-ms treatments and 4.5 ± 0.7 mm^3/min for 10-ms treatments. The lesion of completely ablated tissue was surrounded by a margin, measuring <200 μm, of incompletely ablated tissue. The margin contained regions of intact smooth muscle and collagen fibrils, which is consistent with sparing of fibromuscular elements. Beyond that margin, glandular and fibromuscular elements appeared normal, consistent with viable untreated tissue.

In TEM images of the liquefied lesion content, both treatment protocols revealed discrete regions with loss of cellular structure and indistinguishable cellular components with a gradient of remaining electron-dense matter. However, with 10-ms pulses (Fig. 7b), there were regions where the cellular debris became more condensed and electron dense versus 1-ms pulses (Fig. 7a), which may indicate some thermal effect in the liquefied lesion content (Wang et al. 2018b). In the SEM images, 10-ms pulses produced layers of fibrillar fragments of collagen covered by a thick layer of cell and protein debris, whereas 1-ms pulses resulted in thinner and cleaner fibrillar fragments with discrete globules of cellular and protein remnants.

DISCUSSION

Herein we report successful results after applying BH for mechanical ablation of fresh *ex vivo* human prostatic tissue. BH produced reproducible mechanical homogenization in prostate tissue samples using two pulse parameter sets, which was confirmed by histologic and ultrastructural analysis. BH treatment targeting, progression and outcomes were readily monitored in real time on B-mode and Doppler ultrasound. The presence of BH-generated bubbles resulted in the appearance of a hyperechoic region at the treatment site during each pulse, and mechanical destruction of tissue eliminated tissue scatters, producing a hypoechoic cavity as treatment was completed.

With the longer 10-ms pulses there may have been subtle thermal effects on the liquefied tissue debris seen grossly and on TEM and SEM. As the same high acoustic power output (0.7 kW) used in this study was sufficient to generate BH for both 1- and 10-ms pulses, longer tissue heating for 10 ms and initiation of boiling early within each pulse may have resulted in whitening of the lesion border and specific changes in the liquefied lesion content observed in SEM and TEM images and related to the thermal effect. Further optimization experiments will aim at minimizing the power output required for generating BH lesions with longer pulses and minimizing "dose" requirements for various pulse lengths.

This study builds on prior pre-clinical work developing cavitation cloud histotripsy as a treatment for BPH in which that technique was successfully used for

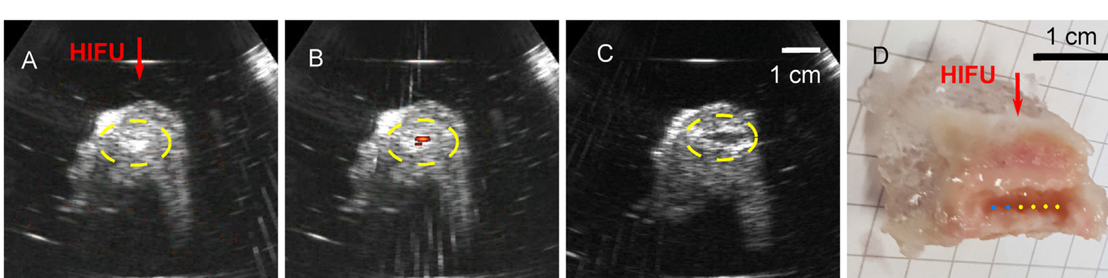

Fig. 5. (a) Appearance of hyperechoic regions on B-mode and (b) power Doppler images during boiling histotripsy (BH) exposures. (c) Hypoechoic appearance of a volumetric lesion of merged BH lesions on B-mode images 15 min after BH exposure. (d) Bisected BH lesion consisting of one line of six discrete foci with 2-mm spacing. Two foci on the left were irradiated with 30 pulses/point (*blue dots*), and four foci on the right with 100 pulses per point (*yellow dots*), resulting in larger lesions. The *red arrow* indicates the direction of BH administration.

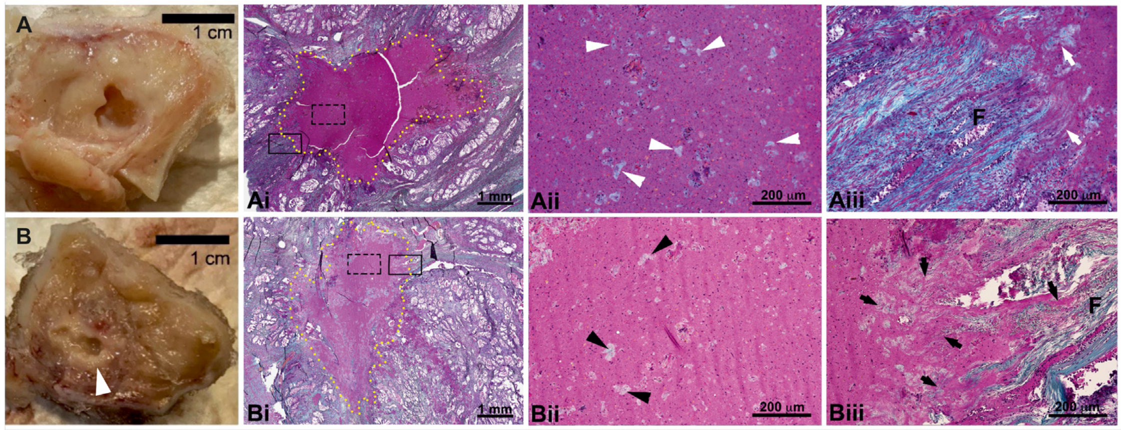

Fig. 6. Gross view (left column) and histologic appearance of Masson's trichrome-stained *ex vivo* human prostate tissue sections treated with (a) 1-ms and (b) 10-ms boiling histotripsy (BH) pulses obtained with 1-mm spacing between foci and 1% duty cycle. (i) Low-power magnification of BH lesions with the lesion border indicated by the *yellow dotted line*. (ii) High-power magnification of the lesion contents (*dashed black box* in i), illustrating uniform ablation for both parameters in the lesion centers with debris <50 μm (*arrowheads*) in size. (iii) High-power magnification of the lesion borders (*solid black box* in i), illustrating an $\sim$200-μm region containing frayed collagen bundles and spared fibromuscular components (*arrowheads*) between the completely ablated lesion and intact untreated tissue containing intact fibrillar collagen (f). The two treatments resulted in varying amounts of homogenization; the 1-ms treatment produced smaller tissue fragments (*white arrowheads*) than the 10-ms treatment, where larger tissue fragments (*black arrowheads*) are present. The border for the 1-ms treatment was more defined compared with that for the 10-ms treatment. The 10-ms treatment resulted in a wide border of frayed collagen fibers (*black arrows*). In contrast, there was a narrower region of frayed collagen fibers at the border (*white arrows*) for the 1-ms treatment. Fibrillar collagen (f) can be observed outside of the lesion.

transabdominal prostate ablation in *in vivo* canine studies (Hall et al. 2009; Hempel et al. 2011; Schade et al. 2012a, 2014) and ultimately led to the creation of a clinical device (Vortx, Histosonics) (Schuster et al. 2018). However, this device failed to produce objective evidence of successful prostate ablation (*e.g.,* change in prostate volume, urine flow rate) (Schuster et al. 2018), and to date, no studies have detailed the effects of the shock scattering approach on human prostate tissue. As a result, this study represents a significant advance in the prostate histotripsy literature by providing definitive evidence of the ability of the BH approach to mechanically ablate human prostate tissue. It also offers the first ultrastructural characterization of the effects of BH on human prostate tissue on both TEM and SEM, confirming that BH can disrupt prostate tissue into subcellular debris. Additionally, similarly to what has been observed in canine prostate with cavitation cloud histotripsy (Hall et al. 2009; Hempel et al. 2011), BH ablation of *ex vivo* human prostate is precise with a $<$200-μm border.

The results presented here were obtained using fresh human *ex vivo* tissue; therefore, the possibility exists that the same BH treatments would not have the same effects in patients. However, several studies by our group have obtained good correlations between *ex vivo* and *in vivo* tissue sensitivities in preclinical models evaluating BH ablation in porcine liver and kidney (Khokhlova et al. 2014, 2019a) and rat kidney (Schade et al. 2019). Additionally, the rapid autopsy tissue collected for these experiments had mechanical properties on SWE imaging similar to those that would be expected clinically in BPH and PCa patients (Barr et al. 2017; Rouvière et al. 2017). Specifically, in young patients without prostatic disorders, the stiffness of the peripheral and central zones ranges from 15 to 25 kPa, whereas the transitional zone exhibits stiffness below 30 kPa. With the development of benign BPH, the peripheral zone remains soft, whereas the transition zone becomes heterogeneous and stiff, with elasticity values ranging from 30 to 180 kPa (Barr et al. 2017). A stiffness value of the peripheral zone greater than 35 kPa is suggestive of a malignancy (Correas et al. 2015; Barr et al. 2017). Wei et al. (2018) reported an even higher stiffness of 82.6 kPa in malignant tumors compared with benign areas. All measurements presented in these articles were performed with an SE12-3 multi-frequency intracavitary probe with an effective 3- to 12-MHz bandwidth. Our studies were performed using an SL15-4 linear array transducer with an effective bandwidth of 4−15 MHz. Thus, the frequency of the transducer we used was similar to the frequency of the transducer used in clinics, and our range of Young's moduli (37.9 $\pm$ 22.2 kPa) measured in the samples was similar to clinical values for benign tissues and certain malignancies. As a result, we anticipate that the observations and developments from this study (with respect to BH pulse parameters) will

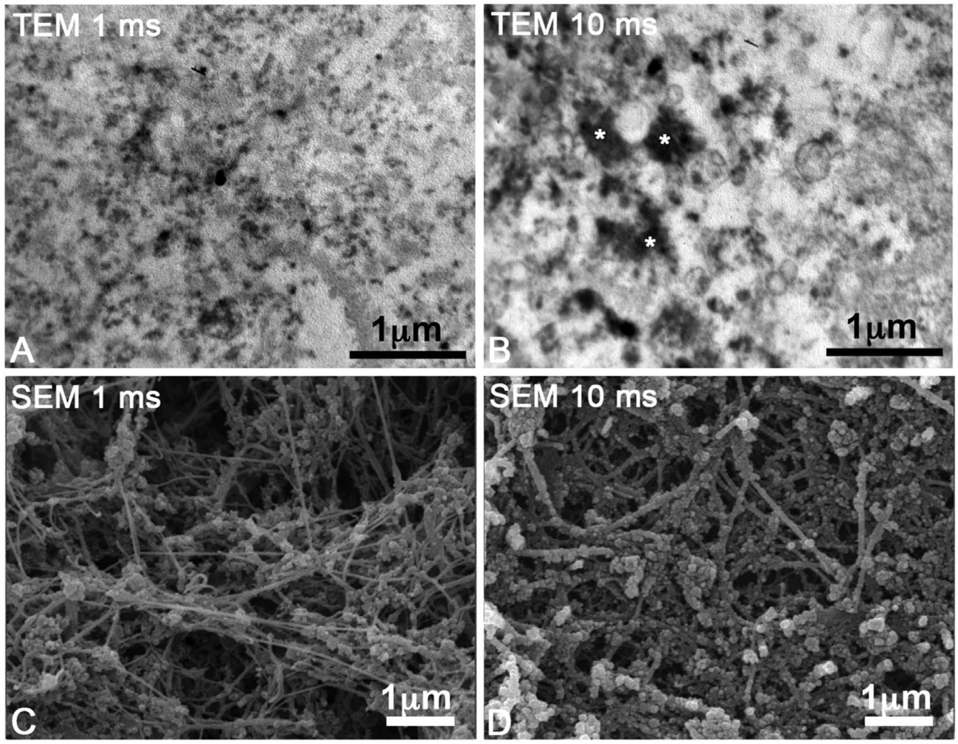

Fig. 7. Transmission electron microscopy (TEM) and scanning electron microscopy (SEM) images of samples taken from boiling histotripsy (BH) lesions produced with 1- and 10-ms pulses. Both treated lesions exhibit loss of cellular structure. With the 10-ms pulses, there are regions where the cellular debris has become more condensed and electron dense (*asterisks*), which may indicate some thermal effect. In SEM images corresponding to the 10-ms pulses, multilayered fragments of fibrillar collagen covered by a thick layer of cell and protein debris were observed, whereas the 1-ms pulse treatment resulted in thinner and cleaner fibrillar fragments with discrete globules of cell and protein remnants.

translate into patients though the optimal BH parameters for clinical prostate ablation remain to be determined.

Prostate cancer tumors and BPH therefore are typically stiffer mechanically (>35 kPa) (Correas et al. 2015; Barr et al. 2017; Wei et al. 2018), compared with normal prostate tissue (from 15 to 30 kPa) (Barr et al. 2017). In previous studies, it was reported that the sensitivity of tissues to histotripsy correlates with their mechanical stiffness and collagenous tissue is more resistant (Vlaisavljevich et al. 2014; Wang et al. 2018b; Khokhlova et al. 2019a, 2019b). Correspondingly, BPH and PCa tissue may have higher resistance to histotripsy; that is, these require a larger number of pulses per focus. Most of the samples used in the experiments contained BPH identified grossly and by palpation, and the BH treatment parameters were sufficient for liquefying them.

Non-thermal ablation with BH offers several potential advantages over existing minimally invasive treatment options for prostate diseases. First, BH's mechanism of action comprising bubbles and mechanical bio-effects enables real-time ultrasound control not possible with other technologies. Second, the precision of BH ablation and lack of heat-sink and thermal diffusion effects (owing to the rapidity of its mechanism) are a major advantage over existing thermal-based techniques (HIFU, cryotherapy, etc.). We anticipate it will enable very tightly controlled ablation near critical structures such as the urinary sphincter and neurovascular bundles to minimize side effects such as urinary incontinence and erectile dysfunction when thinking about PCa focal therapy. Third, as this study demonstrated, refinement of BH pulse parameters enables the tailoring of pulse parameters and bio-effects, acceleration of treatments and facilitation of clinically relevant rates of non-thermal tissue ablation. Collectively, these advantages suggest that BH, unlike any other available minimally invasive therapy for prostate pathology, can be translated into a clinical treatment of prostate diseases.

The positive results of this study, combined with the potential advantages of the BH approach, support further investigation and development of BH for both PCa and BPH. Compared with cavitation cloud histotripsy, BH pulse parameters may be more amenable to miniaturization to facilitate the transrectal application that has been successfully used for thermal HIFU in prostate (Guillaumier et al. 2018; Huber et al. 2020). Indeed, simulations by our group suggested that BH of the prostate is feasible using a probe with a geometry similar to that of existing thermal transrectal HIFU devices (Khokhlova et al. 2018). Following these studies, a pre-clinical system has been developed, and pilot experiments in *ex vivo* and *in vivo* tissue are underway (Schade et al. 2020).

CONCLUSIONS

These data represent successful application of the BH method with real-time B-mode and Doppler-type imaging in fresh *ex vivo* human prostate tissue and suggest that BH can be accelerated without the loss of efficiency using shorter pulses of sufficient shock amplitude (1 ms vs. 10 ms). On the basis of these encouraging results, further evaluation of BH for prostate applications is underway.

Acknowledgments—Funding was provided by National Institutes of Health (NIH) Grants R21CA219793 and R01DK119310; Russian Foundation for Basic Research (RFBR) Grant 17-54-33034; and Russian Science Foundation (RSF) Grant 21-72-00067.

Conflict of interest disclosure—The authors declare no conflicts of interest.

REFERENCES

Barr RG, Cosgrove D, Brock M, Cantisani V, Correas JM, Postema AW, Salomon G, Tsutsumi M, Xu HX, Dietrich CF. WFUMB guidelines and recommendations on the clinical use of ultrasound elastography: Part 5. Prostate. Ultrasound Med Biol 2017;43:27–48.

Canney MS, Khokhlova VA, Bessonova OV, Bailey MR, Crum LA. Shock-induced heating and millisecond boiling in gels and tissue due to high intensity focused ultrasound. Ultrasound Med Biol 2010;36:250–267.

Correas JM, Tissier AM, Khairoune A, Vassiliu V, Méjean A, Hélénon O, Memo R, Barr RG. Prostate cancer: Diagnostic performance of real-time shear-wave elastography. Radiology 2015;275:280–289.

Dubinsky TJ, Khokhlova TD, Khokhlova V, Histotripsy Schade GR. The next generation of high-intensity focused ultrasound for focal prostate cancer therapy. J Ultrasound Med 2020;39:1057–1067.

Duck FA. Physical properties of tissue. 2London: Academic Press; 1990. p. 96–99.

Elhelf IAS, Albahar H, Shah U, Oto A, Cressman E, Almekkawy M. High intensity focused ultrasound: The fundamentals, clinical applications and research trends. Diagn Interv Imaging 2018;99:349–359.

Eranki A, Farr N, Partanen A, Sharma KV, Rossi CT, Rosenberg AZ, Kim A, Oetgen M, Celik H, Woods D, Yarmolenko PS, Kim PCW, Wood BJ. Mechanical fractionation of tissues using microsecond-long HIFU pulses on a clinical MR-HIFU system. Int J Hyperthermia 2018;34:1213–1224.

Gschwend PM, Hintze JM, Herrmann IK, Pratsinis SE, Starsich FHL. Precision in thermal therapy: Clinical requirements and solutions from nanotechnology. Adv Ther 2021;4 2000193.

Guillaumier S, Peters M, Arya M, Afzal N, Charman S, Dudderidge T, Hosking-Jervis F, Hindley RG, Lewi H, McCartan N, Moore CM, Nigam R, Ogden C, Persad R, Shah K, van der Meulen J, Virdi J, Winkler M, Emberton M, HU Ahmed. A multicentre study of 5-year outcomes following focal therapy in treating clinically significant nonmetastatic prostate cancer. Eur Urol 2018;74:422–429.

Hall TL, Hempel CR, Wojno K, Xu Z, Cain CA, Roberts WW. Histotripsy of the prostate: Dose effects in a chronic canine model. Urology 2009;74:932–937.

Hempel CR, Hall TL, Cain CA, Fowlkes JB, Xu Z, Roberts WW. Histotripsy fractionation of prostate tissue: Local effects and systemic response in a canine model. J Urol 2011;185:1484–1489.

Huber PM, Afzal N, Arya M, Boxler S, Dudderidge T, Emberton M, Guillaumier S, Hindley RG, Hosking-Jervis F, Leemann L, Lewi H, McCartan N, Moore CM, Nigam R, Odgen C, Persad R, Thalmann GN, Virdi J, Winkler M, HU Ahmed. An exploratory study of dose escalation. J Endourol 2020;34:641–646.

Khokhlova TD, Canney MS, Khokhlova VA, Sapozhnikov OA, Crum LA, Bailey MR. Controlled tissue emulsification produced by high intensity focused ultrasound shock waves and millisecond boiling. J Acoust Soc Am 2011;130:3498–3510.

Khokhlova TD, Wang YN, Simon JC, Cunitz BW, Starr F, Paun M, Crum LA, Bailey MR, Khokhlova VA. Ultrasound-guided tissue fractionation by high intensity focused ultrasound in an in vivo porcine liver model. Proc Natl Acad Sci USA 2014;111:8161–8166.

Khokhlova VA, Fowlkes JB, Roberts WW, Schade GR, Xu Z, Khokhlova TD, Hall TL, Maxwell AD, Wang YN, Cain CA. Histotripsy methods in mechanical disintegration of tissue: Towards clinical applications. Int J Hyperthermia 2015;31:145–162.

Khokhlova VA, Rosnitskiy PB, Yuldashev PV, Khokhlova TD, Sapozhnikov OA, Gavrilov LR, Karzova MM, Schade GR. Design of a transrectal probe for boiling histotripsy ablation of prostate. Final Program and Abstract Book of the 18th International Symposium on Therapeutic Ultrasound. : Nashville, TN, USA; 2018. p. 67–69.

Khokhlova TD, Schade GR, Wang YN, Buravkov SV, Chernikov VP, Simon JC, Starr F, Maxwell AD, Bailey MR, Kreider W, Khokhlova VA. Pilot in vivo studies on transcutaneous boiling histotripsy in porcine liver and kidney. Sci Rep 2019a;9:20176.

Khokhlova VA, Rosnitskiy PB, Tsysar SA, Buravkov SV, Sapozhnikov OA, Karzova MM, Khokhlova TD, Maxwell AD, Gaifullin NM, Kadrev AV, Okhobotov DA, Kamalov AA, Schade GR. A novel method for non-invasive mechanical ablation of prostate tumors using pulsed focused ultrasound. Urologiia 2019b;6:67–73.

Li T, Chen H, Khokhlova T, Wang YN, Kreider W, He X, Hwang JH. Passive cavitation detection during pulsed HIFU exposures of ex vivo tissues and in vivo mouse pancreatic tumors. Ultrasound Med Biol 2014;40:1523–1534.

Lin KW, Kim Y, Maxwell AD, Wang TY, Hall TL, Xu Z, Fowlkes JB, Cain CA. Histotripsy beyond the intrinsic cavitation threshold using very short ultrasound pulses: Microtripsy. IEEE Trans Ultrason Ferroelectr Freq Control 2014;61:251–265.

Maxwell AD, Wang TY, Cain CA, Fowlkes JB, Sapozhnikov OA, Bailey MR, Xu Z. Cavitation clouds created by shock scattering from bubbles during histotripsy. J Acoust Soc Am 2011;130:1888–1898.

Maxwell AD, Yuldashev PV, Kreider W, Khokhlova TD, Schade GR, Hall TL, Sapozhnikov OA, Bailey MR, VA Khokhlova. A prototype therapy system for transcutaneous application of boiling histotripsy. IEEE Trans Ultrason Ferroelectr Freq Control 2017;64:1542–1557.

Pahk KJ, Gélat P, Sinden D, Dhar DK, Saffari N. Numerical and experimental study of mechanisms involved in boiling histotripsy. Ultrasound Med Biol 2017;43:2848–2861.

Park S, Pham NT, Huynh HT, Kang HW. Development of temperature controller-integrated portable HIFU driver for thermal coagulation. Biomed Eng Online 2019;18:77.

Parsons JE, Cain CA, Abrams GD, Fowlkes JB. Pulsed cavitational ultrasound therapy for controlled tissue homogenization. Ultrasound Med Biol 2006;32:115–129.

Rosnitskiy PB, Yuldashev PV, Sapozhnikov OA, Maxwell AD, Kreider W, Bailey MR, Khokhlova VA. Design of HIFU transducers for generating specified nonlinear ultrasound fields. IEEE Trans Ultrason Ferroelectr Freq Control 2017;64:374–390.

Rouvière O, Melodelima C, Hoang Dinh A, Bratan F, Pagnoux G, Sanzalone T, Crouzet S, Colombel M, Mège-Lechevallier F, Souchon R. Stiffness of benign and malignant prostate tissue measured by shear-wave elastography: A preliminary study. Eur Radiol 2017;27:1858–1866.

Sapozhnikov OV, Tsysar SA, Khokhlova VA, Kreider W. Acoustic holography as a metrological tool for characterizing medical ultrasound sources and fields. J Acoust Soc Am 2015;138:1515–1532.

Schade GR, Hall TL, Roberts WW. Urethral-sparing histotripsy of the prostate in a canine model. Urology 2012a;80:730–735.

Schade GR, Keller J, Ives K, Cheng X, Rosol TJ, Keller E, Roberts WW. Histotripsy focal ablation of implanted prostate tumor in an ACE-1 canine cancer model. J Urol 2012b;188:1957–1964.

Schade GR, Styn NR, Ives KA, Hall TL, Roberts WW. Prostate histotripsy: Evaluation of prostatic urethral treatment parameters in a canine model. BJU Int 2014;113:498–503.

Schade GR, Wang YN, D'Andrea S, Hwang JH, Liles WC, Khokhlova TD. Boiling histotripsy ablation of renal cell carcinoma in the Eker rat promotes a systemic inflammatory response. Ultrasound Med Biol 2019;45:137–147.

Schade GR, Sekar R, Khokhlova TD, Peek A, Wang YN, Totten S, Kreider W, Kumar Y, Sapozhnikov OA, Maxwell AD, Khokhlova VA. Transrectal boiling histotripsy of the prostate: Initial pre-clinical results with a prototype device. 7th International Symposium on Focused Ultrasound. : Washington, DC; 2020. p. 9–13. November.

Schuster TG, Wei JT, Hendlin K, Jahnke R, Roberts WW. Histotripsy treatment of benign prostatic enlargement using the Vortx Rx System: Initial human safety and efficacy outcomes. Urology 2018;114:184–187.

Simon JC, Sapozhnikov OA, Khokhlova VA, Wang YN, Crum LA, Bailey MR. Ultrasonic atomization of tissue and its role in tissue fractionation by high intensity focused ultrasound. Phys Med Biol 2012;57:8061–8078.

Vlaisavljevich E, Kim Y, Owens G, Roberts W, Cain C, Xu Z. Effects of tissue mechanical properties on susceptibility to histotripsy-induced tissue damage. Phys Med Biol 2014;59:253–270.

Wang TY, Xu Z, Winterroth F, Hall TL, Fowlkes JB, Rothman ED, Roberts WW, Cain CA. Quantitative ultrasound backscatter for pulsed cavitational ultrasound therapy—Histotripsy. IEEE Trans Ultrason Ferroelectr Freq Control 2009;56:995–1005.

Wang YC, Chan TC, Sahakian AV. Real-time estimation of lesion depth and control of radiofrequency ablation within ex vivo animal tissues using a neural network. Int J Hyperthermia 2018a;34:1104–1113.

Wang YN, Khokhlova TD, Buravkov S, Chernikov V, Kreider W, Partanen A, Farr N, Maxwell A, Schade GR, Khokhlova VA. Mechanical decellularization of tissue volumes using boiling histotripsy. Phys Med Biol 2018b;63 235023.

Wei C, Li C, Szewczyk-Bieda M, Upreti D, Lang S, Huang Z, Nabi G. Performance characteristics of transrectal shear wave elastography imaging in the evaluation of clinically localized prostate cancer: A prospective study. J Urol 2018;200:549–558.

Xu Z, Hall TL, Vlaisavljevich E, Lee FT. Histotripsy: The first noninvasive, non-ionizing, non-thermal ablation technique based on ultrasound. Int J Hyperthermia 2021;38:561–575.

Yuldashev PV, Karzova MM, Kreider W, Rosnitskiy PB, Sapozhnikov OA, Khokhlova VA. "HIFU Beam:" A simulator for predicting axially symmetric nonlinear acoustic fields generated by focused transducers in a layered medium. IEEE Trans Ultrason Ferroelectr Freq Control 2021;68:2837–2852.

Zhou Y, Cunitz BW, Dunmire B, Wang YN, Karl SG, Warren C, Mitchell S, Hwang JH. Characterization and ex vivo evaluation of an extracorporeal high-intensity focused ultrasound (HIFU) system. J Appl Clin Med Phys 2021;22:345–359.